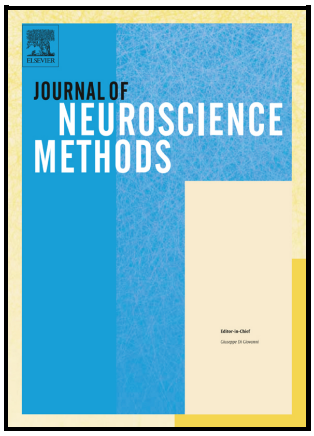

An Adaptive Joint CCA-ICA Method for Ocular Artifact Removal and its Application to Emotion Classification

Xiaohui Gao, Shilai Zhang, Ke Liu, Ziqin Tan, Guanyi Zhao, Yumeng Han, Yue Cheng, Cunbo Li, Fali Li, Yin Tian, Peiyang Li

PII: S0165-0270(23)00060-2

DOI: https://doi.org/10.1016/j.jneumeth.2023.109841

Reference: NSM109841

To appear in: *Journal of Neuroscience Methods*

Received date: 4 February 2023
Revised date: 10 March 2023
Accepted date: 19 March 2023

Please cite this article as: Xiaohui Gao, Shilai Zhang, Ke Liu, Ziqin Tan, Guanyi Zhao, Yumeng Han, Yue Cheng, Cunbo Li, Fali Li, Yin Tian and Peiyang Li, An Adaptive Joint CCA-ICA Method for Ocular Artifact Removal and its Application to Emotion Classification, *Journal of Neuroscience Methods,* (2023) doi:https://doi.org/10.1016/j.jneumeth.2023.109841

An adaptive joint CCA-ICA method for ocular artifact removal and its application to emotion classification

Xiaohui Gao[a,b,c,#], Shilai Zhang[d,#], Ke Liu[e], Ziqin Tan[a,b,c], Guanyi Zhao[a,b,c], Yumeng Han[a,b,c], Yue Cheng[f], Cunbo Li[d], Fali Li[d,*], Yin Tian [a,b,c,*], Peiyang Li [a,b,c,*]

[#] Contributed equally to this work.

[a] the School of Bioinformatics, Chongqing University of Posts and Telecommunications, Chongqing, 400065, China.

[b] Chongqing Institute for Brain and Intelligence, Guangyang Bay Laboratory, Chongqing 400064, China

[c] Institute for Advanced Sciences, Chongqing University of Posts and Communications

[d] the Clinical Hospital of Chengdu Brain Science In-stitute, MOE Key Lab for Neuroinformation and School of Life Science and Technology, University of Electronic Science and Technology of China, Chengdu, 610054, China.

[e] the Chongqing University of Posts and Telecommunications Chongqing Key Laboratory of Computational Intelligence Chongqing, 400065, China.

[f] the Key Laboratory of Intelligent Analysis and Decision on Complex Systems, Chongqing University of Posts and Telecommunications, Chongqing, 400065, China

*Corresponding author1: Peiyang Li; email: pyli@cqupt.edu.cn

*Corresponding author2: Yin Tian; email: tianyin@cqupt.edu.cn

*Corresponding author3: Fali Li; email: fali.li@uestc.edu.cn

Abstract

***Background*:** The quality of Electroencephalogram (EEG) signals is critical for revealing the neural mechanism of emotions. However, ocular artifacts decreased the signal to noise ratio (SNR) and covered the inherent cognitive component of EEGs, which pose a great challenge in neuroscience research.

***New Method*:** We proposed a novel unsupervised learning algorithm to adaptively remove the ocular artifacts by combining canonical correlation analysis (CCA), independent component analysis (ICA), higher-order statistics, empirical mode decomposition (EMD), and wavelet denoising techniques. Specifically, the combination of CCA and ICA aimed to improve the quality of source separation, while the higher-order statistics further located the source of ocular artifacts. Subsequently, these noised sources were further corrected by EMD and wavelet denoising to improve SNR of EEG signals.

***Results*:** We evaluated the performance of our proposed method with simulation studies and real EEG applications. The results of simulation study showed our proposed method could significantly improve the quality of signals under almost all noise conditions compared to four state-of-art methods. Consistently, the experiments of real EEG applications showed that the proposed methods could efficiently restrict the components of ocular artifacts and preserve the inherent information of cognition processing to improve the reliability of related analysis such as power spectral density (PSD) and emotion recognition.

***Comparison with existing methods*:** Our proposed model outperforms the comparative methods in EEG recovery, which further improve the application performance such as PSD analysis and emotion recognition.

***Conclusions*:** The superior performance of our proposed method suggests that it is promising for removing ocular artifacts from EEG signals, which offers an efficient EEG preprocessing technology for the development of brain computer interface such as emotion recognition

Keywords: Electroencephalogram, blind source separation, ocular artifact removal, emotional classification.

1.Introduction

In recent years, EEG-based analysis has gained increasing attention in neuroscience research. However, artifacts such as electromyogram (EMG), electrocardiogram (ECG), and electrooculogram (EOG) during EEG recordings negatively impacts the representation of the inherent information of the brain [1, 2]. Among these artifacts, ocular artifacts can be particularly problematic, as they are common biological phenomena that may lead to incorrect analysis [3]. This has caused widespread concern regarding the impact of ocular artifacts on neural mechanism decoding in neuroscience research. Therefore, removing these artifacts is essential to improve the accuracy of neural mechanism decoding and deepen our understanding of brain function.

Traditional methods to remove ocular artifacts typically rely on mapping signals from time to frequency domain [4]. However, this method would result in loss of information due to spectral overlap between neural activity and artifact noise. Moreover, another feasible approach for artifact removal were regression-based methods, but it's worth noting that these methods require the recording of the EOG channels [3], and might lead to serious signal distortion when the reference channels are noisy [1]. Compared to these two methods, BSS-based methods, such as principal component analysis (PCA) [5], ICA [6], and CCA [1, 3] have shown better performance in separating the components of artifacts and neural activity. Among these methods, zeroing-ICA (ZICA), as a widely used method, removed artifacts by calculating the independent component vector and setting a hard threshold for the recognition and suppression of artifacts [7, 8]. However, their performance heavily relies on subjective judgment of the threshold designed [1]. In addition, some adaptive methods have been proposed to alleviate the problem [1, 6]. Castellanos et al. developed a novel method that combined the wavelet decomposition with ICA (WICA) to detect and remove artifacts automatically, in which method could detected and removed multiple types of ocular artifacts automatically based on wavelet soft-threshold [6]. Li et al. introduced the clustering method into ICA to propose a novel artifacts removal method that combined clustering technology and local density, this method utilized the density distribution of the components in the data sample to distinguish the noise components from the signal

components, so as to adaptively determine the threshold and distinguish the noise in the components [1]. Maddirala et al. developed a new framework which combined ICA with continuous wavelet transform, *k*-means and singular spectrum analysis method, adopted the cluster after *k*-means clustering as the input signal, and used an adaptive threshold in ICA decomposition to detect and remove eye-blink artifacts [9]. However, these studies failed to consider cooperative oscillation patterns of ocular artifacts among multiple EEG channels that which might lead to loss of information of normal neural activity [10, 11].

To solve this problem, many researchers have tried various methods [3, 9, 12]. For example, Mahajan et al. utilized higher-order features such as multiscale sample entropy and kurtosis to identify noisy channels, and combined them with wavelet independent component analysis to develop an unsupervised technique for removing ocular artifacts from EEG signals [3]. Similarly, Chen et al. proposed a method using multivariate EMD (M-EMD) and BSS technology to remove artifacts from few-channel EEG recordings, achieving effective noise removal in the case of limited channels [12]. Essentially, these methods automatically identify channels affected by artifacts and remove corresponding artifact components, mitigating the loss of valuable EEG information. As a result, they provided a reference approach for analyzing few-channel EEG signals.

Additionally, CCA-based methods have been widely used for artifact removal due to their superior performance in artifact detection [12-16]. CCA can utilize the correlation between signals and noise components to better distinguish them, and it performs better when dealing with EEG signals from fewer channels [12, 17, 18]. Because the decomposition principles of these BSS techniques are different, the EEG components separated by each method may also different [19-22]. Specifically, CCA can use the linear correlation between EEG and EOG signals to separate ocular artifacts in EEG signals [12, 15, 19], while ICA can perform independent component analysis on EEG signals and use the independence and non-Gaussian of signals to separate eye movement artifacts [23-25]. Based on the characteristics of different methods and the statistical properties of EEG and EOG signals, it is possible to achieve more accurate separation of ocular artifacts in EEG signals without relying on other physiological signals or specific testing conditions by integrating CCA and ICA methods.

In this paper, we proposed a novel automated ocular artifacts removal method that combined the CCA, ICA, automatic ocular artifact detection, EMD-based single-channel decomposition technique and ICA-based wavelet denoising. That is, the proposed method was adapted to identify noisy component channels and retain more neural activity-related components. The main contributions of this paper were summarized as follows:

1) The proposed method separated the artifacts and intrinsic neural components accurately.
2) The proposed method retained more neural activity-related components by adaptively identifying noisy component channels and performing denoising analysis on the selected components.

The remainder of this paper was organized as follows. Section Method introduced the algorithmic principles of the proposed method and the definition of simulation and real EEG applications. Section Result illustrated the comparison results of simulation and real EEG applications among these methods. Section Discussion analyzed the performance difference between different methods and the possible superiority of our proposed method. Section Conclusion presented our findings in this work briefly.

2.Materials and methods

A. the adaptive artifacts removal tool for fewer component channels by Joint independent analysis (FCCJIA)

This part described a fully automated model that was designed for more effective separation of noise components, determination and analysis of channels with noisy components, and removal of artifact components. Specifically, the following four parts provided a detailed description of the implementation of the model.

A.1. Joint independent analysis for component decomposition

We mainly combined ICA with CCA to enhance the performance of artifacts removal for EEG-based analysis. The classical pattern of CCA had the following form:

$$X = A_{CCA} \times S_{CCA} \tag{1}$$

where $X \in R^{D \times N}$ denoted observed signal, D denoted the dimension of time series and N represented the series length. The $A_{CCA} \in R^{D \times S1}$ and $S_{CCA} \in R^{S1 \times N}$ denoted the confusion matrix and the source ingredient matrix respectively. Moreover, the ICA [26] was further utilized in S_{CCA} to extract the independent components (ICs) of artifacts, i.e.,

$$S_{CCA} = A_{ICA}^{*} \times S_{ICA}^{*} \tag{2}$$

where $A_{ICA}^{*} \in R^{S1 \times S2}$ and $S_{ICA}^{*} \in R^{S2 \times N}$ denoted the confusion matrix and the source ingredient matrix estimated by ICA, respectively. Therefore, equation (1) could be further expressed as

$$X = A_{CCA} \times \left(A_{ICA}^{*} \times S_{ICA}^{*} \right) \Rightarrow A^{\Xi} \times S_{ICA}^{*} \tag{3}$$

$$A^{\Xi} = A_{CCA} \times A_{ICA}^{*} \tag{4}$$

Generally, the equations mentioned above mainly separated the source components between signals and artifacts within the canonical correlation subspace while preserving the independent characteristics among these components.

A.2. Selection and analysis of noisy component channel

The distribution of ocular artifacts presented high positive kurtosis [3, 27]. Therefore, considering that kurtosis is the fourth-order cumulant that can be used to measure the peak distribution of random variables [3], we used kurtosis as a marker to represent the ocular artifacts and achieved the selection of the noisy component channel.

$$kurtosis = m_4 - 3m_2^2 \tag{5}$$

$$m_n = E\{(S^*_{ICA,i} - m_1)^n\} \tag{6}$$

where m_n, m_1 and E denoted the n-th order central moment of the variable, mean, and the expectation function, respectively [3, 23]. Then, the identified single noisy channel was decomposed into multiple components using EMD, which further facilitated denoising analysis for fewer component channels in a more convenient way. Specifically, EMD was represented as

$$Sig = \sum_{i=1}^{n} IMF_i + Res \tag{7}$$

where Sig uniformly denoted as the noisy component channel, IMF_i represented the i-th intrinsic mode function, and Res denoted the residual. In addition, the terminate condition of the iterative of EMD process should satisfy the following form:

$$SD = \left|Env^{k-1} - Env^{k}\right|^2 \Big/ \left(Env^{k-1}\right)^2 \le \upsilon \tag{8}$$

where Env^k denoted the mean value of the upper and lower envelope of the k-th IMF component, and the iteration process would be stop when SD less than the threshold υ.

A.3. Artifact removal by ICA-based wavelet denoising

Based on the *IMFs* obtained by EMD, we further utilized ICA and wavelet denoising to remove ocular artifact components with the following steps:

1) Evaluated the discrete wavelet transform decomposition of the identified artifacts ingredients.
2) Defined the threshold K and judged the wavelet coefficient, i.e., if the coefficient exceeded the threshold, the coefficient was set to 0.

$$K = \sqrt{2\log N} \cdot median\left(\left|W\left(j,k\right)\right| / 0.6745\right) \tag{9}$$

where W denoted the wavelet coefficient, and the constant 0.6745 represented the wideband neuronal signal for Gaussian noise [3, 6].

3) Computed the inverse discrete wavelet transform of the thresholded coefficients and recombined the components consisting of neuronal activity.
4) Rebuilt the EEG signal by inverse-transformed wavelet coefficients.

In general, the complete flow chart of this method could be represented as in Fig. 1.

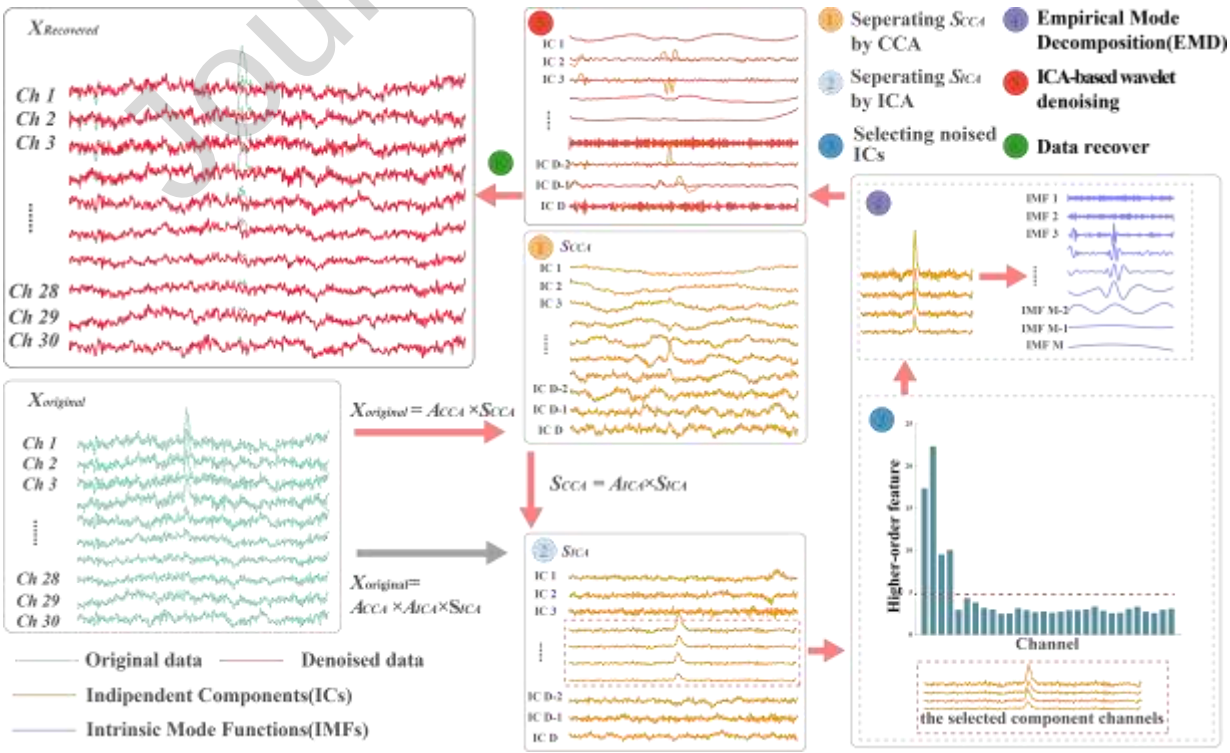

Fig. 1. the flow chart of the proposed method.

B. Computational complexity

The time complexity of the proposed algorithm mainly consists of following aspects, including joint independent analysis, EMD and ICA-based wavelet denoising. Specifically, the time complexity of CCA was primarily attributed to the matrix decomposition with SVD, which had a time complexity of $O(D^2\times N^2)$. Meanwhile, the component matrix obtained from CCA needed to be further processed by ICA, which had a time complexity mainly attributed to iterative computation, with a time complexity of $O(S1\times N^3)$. In addition, the EMD algorithm used for noisy channel analysis had a time complexity of $O(N)$, while the time complexity of wavelet denoising ICA was $O(N^2)$. Therefore, the overall time complexity of the algorithm could be summarized as $O(D^2\times N^2+S1\times N^3+c\times(N+N^2))$, where c denoted the selected component channels.

C. Experiments

Subsequently, to quantitatively evaluate the performance of FCCJIA in resisting ocular artifacts, a series of advanced methods were applied for comparison. The method named ZICA mentioned in [1, 3] was adopted as the baseline method. The wavelet enhanced independent component analysis named as WICA proposed in [6], the adaptive threshold independent component analysis (ATICA) proposed in [1], and the adaptive artifact channels selection and denoising by multiscale sample entropy, kurtosis, and wavelet-ICA (MEICA) proposed in [3] were also used. In addition, an evaluation experiment consisting of simulation studies and real EEG applications was utilized. During the simulation studies, we focused on the influence of simulated noise on the signal recovery performance under various conditions. Specifically, we mainly discussed the method's effectiveness by artifact occurrence rates and influenced channels in succession. Furthermore, the comparison indexes were further utilized to verify the performance of artifact removal. For real EEG applications, we mainly validated its effectiveness and reliability under ocular artifacts through two aspects: 1) evaluation metrics that contained the correlation coefficient and mutual information; 2) emotion classification based on the feature of power spectral density.

C.1. Simulation study

In this section, we mainly assessed the influence of two types of noise on five ocular artifact removal methods. During the simulation study, we collected 4 trials of 30-channel EEG segments with 1000 time points without noise (the collection method was the same as described in **Dataset-1**). These data were used to evaluate the denoising performance of our proposed method under the two types of noise, outliers and ocular artifacts, respectively. Additionally, to analyze the performance differences among these methods, we conducted two comparative experiments to evaluate the performance of our method under different noise conditions: 1) the influence of occurrence rate (OR), $OR\in[0.4\%,0.5\%,0.6\%,0.7\%,0.8\%]$; 2) the influenced time series (ITS) that were contaminated by noises, $ITS\in[6,7,8,9,10]$. Moreover, the noise addition operation for the two types of noise could be described as follows.

• ***Noise category***-*Outlier addition*

$$X_{k,i}^{noise}=X_{k,i}+\varepsilon_{k,i},\varepsilon_{k,i}\sim\begin{cases}N\left(20\cdot\mathrm{var}\left(X_{k,\cdot}\right),1\right), w.p.\ OR\\ N(0,0) \quad , w.p.\ 1-OR\end{cases} \tag{10}$$

where $X_{k,i}^{noise}$ indicated the noisy data after artifacts addition for the k-th time series at the time point i, $X_{k,i}$ denoted the collected data without outliers, $\varepsilon_{k,i}$ represented the additional noise of outlier.

• ***Noise category***-*Ocular artifact addition*

$$X_{k,i\to i+24}^{noise}=X_{k,i\to i+24}+\Sigma,\Sigma\sim\begin{cases}OcularArtifact, w.p.\ OR\\ 0 \quad , w.p.\ 1-OR\end{cases} \tag{11}$$

where $X_{k,i\to i+24}^{noise}$ indicated the noisy data after artifacts addition for the k-th time series within the time period from i to j, $X_{k,i\to i+24}$ denoted the collected data without ocular artifacts, $\Sigma\in R^{1\times 25}$ represented the additional ocular artifacts.

In current study, we mainly utilized the EEGs recorded in the channels of frontal aera, because this aera has been reported to be seriously influenced by ocular artifacts [28-31]. Specifically, the channels to add simulated ocular artifacts were randomly selected and the occurrence of the ocular artifacts is also set randomly. The complete simulation steps could be referred to Fig. 2, and the detailed process was described as follows.

Step-1: Simulated different noise conditions as mentioned before, i.e., 1) the influence of noise occurrence rates; 2) the influenced time series that contaminated noises.

Step-2: Removed the ocular artifacts by methods.

Step-3: Evaluated the performance by the following indexes among methods, which included:

• ***Index***-1: Computed the SNR as the following formula [1, 32]

$$SNR=\frac{1}{Ch}\cdot\sum_{k=1}^{Ch}10\cdot log\frac{\sum_{i=1}^{N}\left(X_{k,i}^{exp}\right)^2}{\sum_{i=1}^{N}\left(X_{k,i}^{exp}-X_{k,i}^{rec}\right)^2} \tag{12}$$

• ***Index***-2: Computed the root mean-square error (RMSE) between recovered data by methods and expected data [33, 34].

$$RMSE = \frac{1}{Ch} \cdot \sum_{k=1}^{Ch} \sqrt{\frac{1}{N} \cdot \sum_{i=1}^{N} \left(X_{k,i}^{exp} - X_{k,i}^{rec} \right)^2} \tag{13}$$

where X^{exp} denoted the expected data and X^{rec} denoted the recovered data by methods.

Step-4: Repeated **Steps 1-3** 100 times under noise conditions to reveal the differences by paired-*t* test [2, 35].

In addition, we investigated the denoising performance of various methods under the influence of stronger noise frequencies, with the noise frequency range adjusted from the original 0.4%~0.8% to 1.2 %~1.6 % (including noise types such as outliers and ocular artifacts). Similarly, the results indicated that our proposed method could significantly improve denoising performance even under strong noise frequency interference. Specific results and design details can be found in the *Appendix. A.*

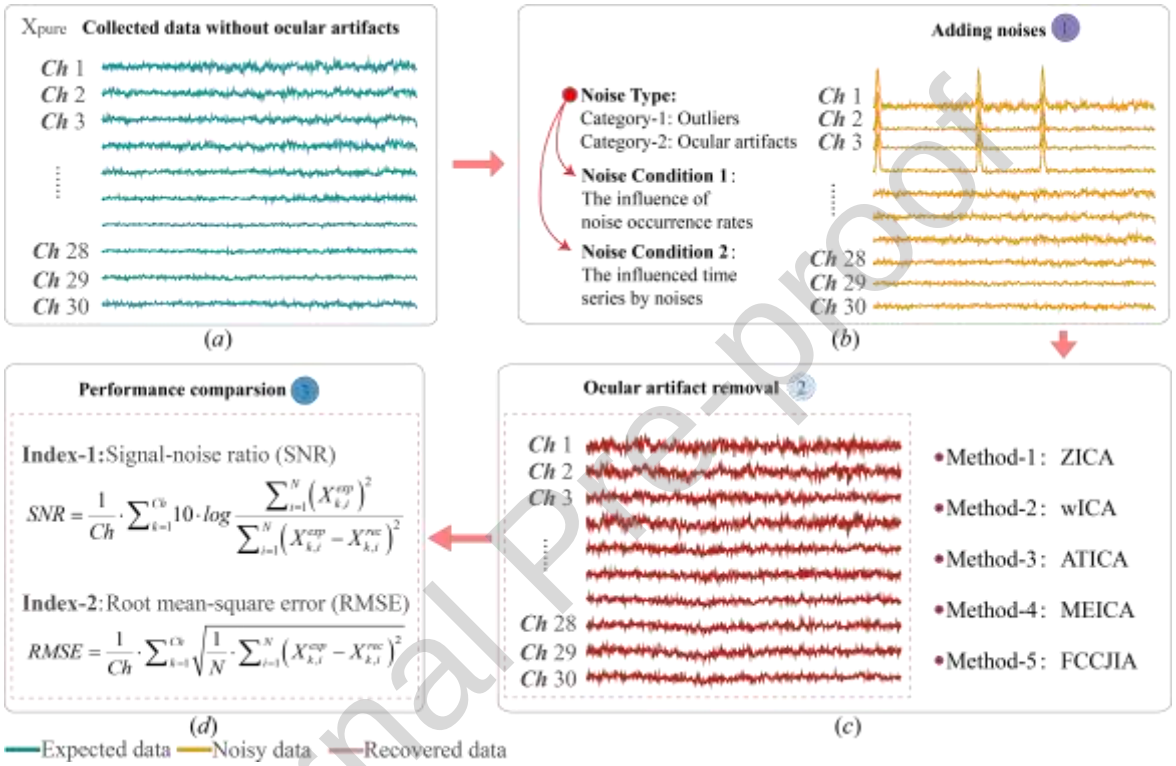

Fig. 2. The complete simulation experiments. (*a*) is the original data without ocular artifacts; (*b*) denotes the several patterns for noise addition; (*c*) is the artifacts denoising by methods; (*d*) is the performance comparisons by methods under two indexes.

C.2. Real EEG Applications

In real EEG analysis, the ocular artifacts introduced by eye blinking were inevitable and usually held a large amplitude, which could bring more complex noises than outliers and the simulated artifacts [2, 35-37]. Thus, in this section, we mainly focused on evaluating the different performance of the aforementioned methods when they were applied to EEG denoising that contained ocular artifacts.

C.2.1. Data description

In the current study, we adopted resting-state data and emotion data with obvious ocular artifacts as the analysis basis for real data. The corresponding description of the datasets was as follows:

Dataset-1: This dataset was recorded from subjects when they were taking resting-state experiments by Neuracle amplifier (Neural Wireless EEG/ERP) that contained 30 Ag/AgCl electrodes (obeyed 10-20 international electrode system), whose system online held a sampling rate of 1000 Hz and 0.5-70 Hz bandpass filter. During experiments, the subjects were required to keep relaxed and blinking naturally, in an enclosed, quiet and well-lit room. In total, 33 trials were selected (each trail was 10-second long) that contained obvious electrical artifacts from 5 participants (2 females, age 20-23) [1]. Specifically, this dataset was utilized to evaluate the performance for artifact removal. Fig. 3 (*a*) showed more details about the experimental design. Especially, the reference EEG segments utilized in the simulation part were collected in the same environment.

Dataset-2: This data was recorded in an EEG based emotional experiment, and its detailed information could be referred to in [2]. In order to elicit different emotional states, a video-based emotion elicitation experiment was designed [2, 38]. In total, 9 film clips were selected and these clips corresponded to positive, neutral, and negative emotions (i.e., there were 3 blocks in total, and each block contained 3 film clips that corresponded to positive, neutral, and negative respectively). In addition, the duration of each film clip was about 3~4 minutes [2]. In general, our previous work adopted 9 healthy college

students with normal or corrected-to-normal vision (4 males; aged 20±1.32), and the experimental protocol was approved by the Institution Research Ethics Board of the Chongqing University of Posts and Telecommunications. The equipment and parameter setting of this experiment were the same as those in Dataset-1. Subsequently, a 200-second EEG segment (within a duration of [10, 210] seconds after the onset of the movie clip) was extracted for further analysis. For each EEG segment, we divided them into subsegments through a shifting window with a length of 10 seconds. Fig. 3 (*b*) showed more details about the experimental design.

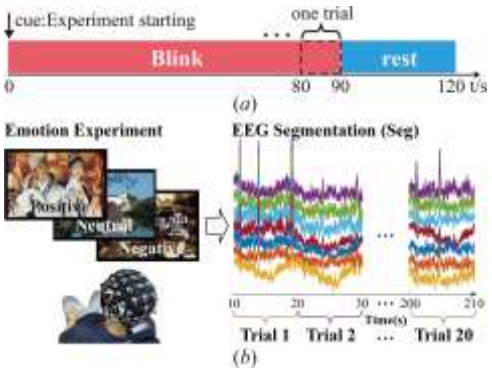

Fig. 3. Timeline for task experiments. (*a*) ocular artifacts task; (*b*) EEG-based emotion experiment.

C.2.2. Preprocessing

Before ocular artifacts removal, the following preprocessing steps were adopted: 1) detrended EEG data and removed the means for each trail; 2) downsampled the EEG trials to 100 Hz.

C.2.3. Performance Measures

For real EEG applications, there no standard criteria to evaluate the performance [2, 35]. Therefore, based on the recovered signals, we adopted two indexes to compare the performance differences among methods. As mentioned in [1, 3], we separately calculated correlation coefficient (*CC*) [39, 40] and mutual information (*MI*) [3, 40, 41] to evaluate the denoising effectiveness of methods based on the **Dataset-1**. Moreover, we further adopted classification accuracies that within subject as the third index to evaluate the ocular artifacts removal performance within **Dataset-2**. i.e.,

• ***Index*-1:** *CC*

CC was utilized to measure the relationship among the signals before and after artifacts removal. The CC_i between the *i-th* channel of the original EEG data x_i and the recovered data y_i could be defined as

$$CC_i = cov(x_i, y_i) / \sigma_{x_i x_i} \sigma_{y_i y_i} \tag{14}$$

where $cov(\cdot)$ represented the co-variance between x_i and y_i by methods, $\sigma_{(\cdot)}$ denoted the variance of the signal itself. Obviously, the average *CC* value between x_i and y_i could be calculated as the following:

$$CC = \frac{1}{N_C} \sum_{i=1}^{N_C} CC_i \tag{15}$$

The *CC* value close to one indicated a good removal of ocular artifact from the EEG data.

• ***Index*-2:** *MI*

MI was the measurement of mutual dependence (amount of information) between x_i and y_i. Given a discrete random variable *X* that had $[x_1, x_2, \cdots, x_N]$ random states with probability distribution of $[p_x(x_1), p_x(x_2), \ldots, p_x(x_N)]$, according to concept of Shannon's entropy, the information entropy of random *X* could be defined as

$$H(X) = -\sum_{n=1}^{N} p_x(x_i) \log_2 p_x(x_i) \tag{16}$$

Similarly, the information entropy of random *Y* could be defined the same with the form mentioned in (16), where $p_x(x_i)$ represented the probability distribution function of *i-th* random state of *X*. Therefore, the joint Shannon's entropy of *X* and *Y* could be represented as

$$H(X,Y) = -\sum_{i=1}^{N} p_{xy}(x_i, y_i) \log_2 p_{xy}(x_i, y_i) \tag{17}$$

where $p_{xy}(x_i, y_i)$ was the joint probability function of *X* and *Y*. In general, the mutual information of two channel signals could be formulated as

$$MI(X,Y) = H(X) + H(Y) - H(X,Y) \tag{18}$$

• ***Index*-3:** Classification accuracy

To avoid the influence of subject differences, we mainly utilized the subject-dependent protocol. During the classification experiment, the power spectral density (PSD) [42] was adopted as features for emotion classification. Both the original EEG

that was contaminated by strong ocular artifacts and the EEG preprocessed with artifact removal by different methods were utilized for comparison. For feature processing, the *z-score* normalization [43] would be applied to features in each trial. Additionally, we adopted the support vector machine (SVM) with a linear kernel as the classifier [44], and the leave-one-block-out validation (LOTO-CV) procedure was utilized according to following previous studies [45, 46]. Finally, we calculated the average classification accuracy across blocks within each subject to reveal the performance differences between the different methods.

3.Results

A. simulation studies

The results of simulation study under the influence of outliers and ocular artifacts were integrated into Tables I to IV, which used two indicators, SNR and RMSE, to measure the results. It was important to note that values in bold indicated the best results, while "∗" denoted a significant difference ($p < 0.05$) between the proposed method and the other methods.

A.1. the influence of occurrence rates

To analyze the influence of the occurrence rate of outliers and ocular artifacts, we increased the occurrence rate of noise from 0.4% to 0.8% with a step size of 0.1%. The number of contaminated time series was defined as 4. Especially, the outlier intensity was defined as 20 times the maximum amplitude in the corresponding time series as the same as defined in (10). The SNR and RMSE in this experiment about two types of noises were integrated into Table I and Table II, respectively. Overall, as the frequency of the noise increased, the proposed method consistently showed a significant improvement in performance for both outliers and ocular artifacts. This to some extent demonstrated the stability and reliability of the FCCJIA method in denoising complex noise interference.

TABLE I
RESULTS COMPARISON WITH INCRASING OCCURRENCE FREQUENCIES OF OUTLIERS

	Frequency of outliers									
	0.4%	0.5%	0.6%	0.7%	0.8%	0.4%	0.5%	0.6%	0.7%	0.8%
	Index value of SNR					Index value of RMSE				
ZICA	10.82 ±0.78∗	10.75 ±0.85∗	10.77 ±0.85∗	10.51 ±1.00∗	10.45 ±1.12∗	0.78 ±0.35∗	0.78 ±0.40∗	0.78 ±0.36∗	0.85 ±0.43∗	0.87 ±0.45∗
WICA	7.41 ±1.52∗	7.25 ±1.41∗	7.40 ±1.51∗	7.33 ±1.50∗	7.30 ±1.36∗	1.05 ±0.15∗	1.01 ±0.13∗	1.03 ±0.14∗	1.02 ±0.14∗	0.99 ±0.14∗
ATICA	9.06 ±1.93∗	8.96 ±1.77∗	9.09 ±1.80∗	9.06 ±1.89∗	9.09 ±1.82∗	0.88 ±0.20∗	0.84 ±0.17∗	0.86 ±0.19∗	0.85 ±0.18∗	0.82 ±0.17∗
MEICA	13.54 ±2.73∗	13.68 ±2.79∗	13.03 ±2.70∗	13.40 ±2.97∗	13.60 ±2.98∗	2.31 ±0.71∗	2.41 ±0.74∗	2.75 ±0.88∗	2.81 ±0.91∗	2.88 ±0.93∗
FCCJIA	**35.13 ±4.51**	**34.31 ±4.13**	**34.89 ±4.05**	**34.11 ±3.75**	**34.85 ±4.48**	**0.17 ±0.45**	**0.15 ±0.35**	**0.19 ±0.51**	**0.19 ±0.47**	**0.25 ±0.57**

TABLE II
RESULTS COMPARISON WITH INCRASING OCCURRENCE FREQUENCIES OF OCULAR ARTIFACTS

	Frequency of ocular artifacts									
	0.4%	0.5%	0.6%	0.7%	0.8%	0.4%	0.5%	0.6%	0.7%	0.8%
	Index value of SNR					Index value of RMSE				
ZICA	8.73 ±0.50∗	8.73 ±0.56∗	8.50 ±0.48∗	8.50 ±0.50∗	8.42 ±0.53∗	1.38 ±0.16∗	1.45 ±0.14∗	1.53 ±0.15∗	1.61 ±0.16∗	1.72 ±0.25∗
WICA	7.04 ±1.31∗	7.08 ±1.47∗	6.92 ±1.20∗	6.98 ±1.56∗	6.63 ±1.49∗	1.07 ±0.16∗	1.06 ±0.15∗	1.07 ±0.15∗	1.09 ±0.15∗	1.16 ±0.17∗
ATICA	8.67 ±1.69∗	8.82 ±1.87∗	8.60 ±1.52∗	8.56 ±1.87∗	8.03 ±1.81∗	0.90 ±0.18∗	0.87 ±0.15∗	0.90 ±0.18∗	0.93 ±0.18∗	1.02 ±0.20∗
MEICA	13.81 ±2.37∗	13.50 ±2.23∗	13.20 ±2.24∗	12.50 ±2.01∗	12.17 ±2.14∗	1.44 ±0.20∗	1.57 ±0.20∗	1.72 ±0.23∗	1.89 ±0.21∗	2.01 ±0.22∗
FCCJIA	**24.78 ±4.45**	**23.74 ±5.27**	**23.27 ±5.45**	**21.94 ±5.09**	**21.24 ±4.88**	**0.41 ±0.36**	**0.50 ±0.44**	**0.50 ±0.39**	**0.55 ±0.44**	**0.58 ±0.42**

A.2. the influenced time series that contaminated by noises

To analyze the number of time series contaminated by noise, we increased the number of noisy time series from 6 to 10 with a step size of 1. The number of noise occurrence rate was kept as 0.3%, and the outlier intensity was defined as 20 times the maximum amplitude in the corresponding time series especially for outlier influenced. The experimental results under the influence of outliers and ocular artifacts were integrated in Table III and Table IV, respectively.

TABLE III
RESULTS COMPARISON WITH INCRASING NUMBERS OF OUTLIERS CONTAMINATED TIME SERIES

	Number of influenced channels									
	6	7	8	9	10	6	7	8	9	10
	Index value of SNR					Index value of RMSE				
ZICA	10.78 ±0.71∗	10.69 ±0.83∗	10.68 ±1.13∗	10.61 ±1.27∗	10.78 ±1.26∗	0.72 ±0.27∗	0.76 ±0.32∗	0.78 ±0.43∗	0.78 ±0.48∗	0.76 ±0.41∗

WICA	7.16 ±1.29*	7.31 ±1.37*	7.36 ±1.46*	7.26 ±1.43*	7.44 ±1.52*	1.04 ±0.17*	1.05 ±0.16*	1.03 ±0.15*	1.01 ±0.13*	1.02 ±0.13*
ATICA	8.84 ±1.84*	8.93 ±1.80*	9.10 ±1.79*	8.92 ±1.89*	9.07 ±2.00*	0.87 ±0.20*	0.88 ±0.18*	0.86 ±0.23*	0.84 ±0.17*	0.85 ±0.16*
MEICA	12.05 ±3.03*	11.03 ±2.77*	10.17 ±2.61*	9.51 ±2.31*	8.26 ±2.43*	2.68 ±0.82*	2.95 ±0.83*	3.12 ±0.85*	3.32 ±0.84*	3.76 ±1.08*
FCCJIA	**34.62 ±4.55**	**34.43 ±4.05**	**33.95 ±3.84**	**33.24 ±3.35**	**32.83 ±2.79**	**0.25 ±0.71**	**0.28 ±0.72**	**0.28 ±0.80**	**0.36 ±0.88**	**0.19 ±0.58**

TABLE IV

RESULTS COMPARISON WITH INCRASING NUMBERS OF OCULAR ARTIFACTS CONTAMINATED TIME SERIES

	Number of influenced channels									
	6	7	8	9	10	6	7	8	9	10
	Index value of SNR					Index value of RMSE				
ZICA	7.77 ±0.46*	7.17 ±0.53*	6.54 ±0.55*	6.03 ±0.58*	5.52 ±0.69*	1.56 ±0.14*	1.71 ±0.14*	1.89 ±0.14*	2.02 ±0.13*	2.20 ±0.12*
WICA	6.99 ±1.22*	7.04 ±1.52*	7.06 ±1.37*	6.98 ±1.52*	7.03 ±1.43*	1.05 ±0.15*	1.03 ±0.15*	1.07 ±0.17*	1.05 ±0.14*	1.09 ±0.15*
ATICA	8.56 ±1.69*	8.47 ±1.86*	8.72 ±1.59*	8.50 ±1.76*	8.71 ±1.78*	0.89 ±0.18*	0.88 ±0.18*	0.89 ±0.18*	0.89 ±0.18*	0.91 ±0.17*
MEICA	12.24 ±1.97*	10.93 ±1.86*	9.97 ±1.96*	9.12 ±1.81*	8.64 ±1.86*	1.68 ±0.22*	1.99 ±0.22*	2.22 ±0.27*	2.45 ±0.29*	2.70 ±0.33*
FCCJIA	25.36 ±3.82	24.68 ±3.70	23.21 ±2.87	22.44 ±3.12	21.99 ±3.45	0.44 ±0.44	0.46 ±0.39	0.51 ±0.54	0.58 ±0.65	0.52 ±0.29

Similar to the results presented in Tables I and II, the FCCJIA method consistently exhibited significant performance improvements compared to other methods, even when more channels were contaminated with noise. Through these simulation studies, we mainly compared the performance of the aforementioned methods under several noise conditions. Tables I to IV provided a brief reference and a comparative analysis of the denoising performance of various methods under the influence of different noise conditions. Based on these results, we found that, regardless of the noise condition, the FCCJIA method consistently showed the best performance in removing ocular artifacts when compared to other methods. In Fig. 4, denoising performance comparisons in one trial were shown, which indicated that the proposed method had the best performance in detecting and removing artifacts. Furthermore, Fig. 5 illustrated a comparison of the power spectra of different methods in noisy and noiseless channels. It could be observed that the signal recovered by FCCJIA was closest to the expected one in terms of power spectrum in the noisy channel. Specifically, the proposed method captured the inherent varying trend of the time series that contained noises and significantly reduced the influence of outliers. Moreover, considering the selection strategy of the noisy channel in FCCJIA, it allowed for the maximum preservation of the normal signal components in the noise-free channel, thereby avoiding the loss of information. That is, the proposed method showed the best performance in waveform fitting among these methods, where the clean EEG channels showed extreme similarity between the expected data and the recovered data. Undoubtedly, the characteristics of FCCJIA, such as noise channel identification and specific channel denoising, were reflected in the evaluation metrics described in Tables I to IV, which was due to the nature of the proposed method and its effects on denoising performance. On the contrary, the ocular-artifact-removal effect of other methods was not satisfactory, with more noise components being preserved. Therefore, we could see that the proposed method could better restrict the ocular artifact influence, which held the capability of selecting noisy component channels, focused more on separating the artifacts and normal neural components, and held the better effect on information retention within the noiseless channel.

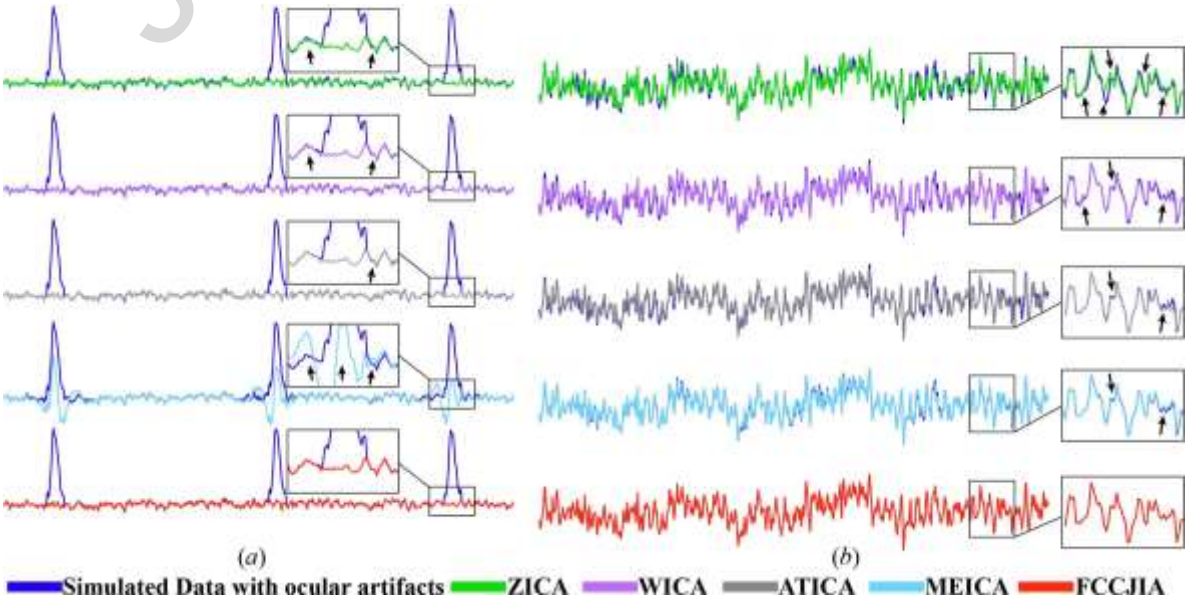

Fig. 4. The comparison of denoising performance among methods within simulated data. (*a*) is the denoising results by methods for noisy channel; (*b*) is the denoising results by methods for noiseless channel

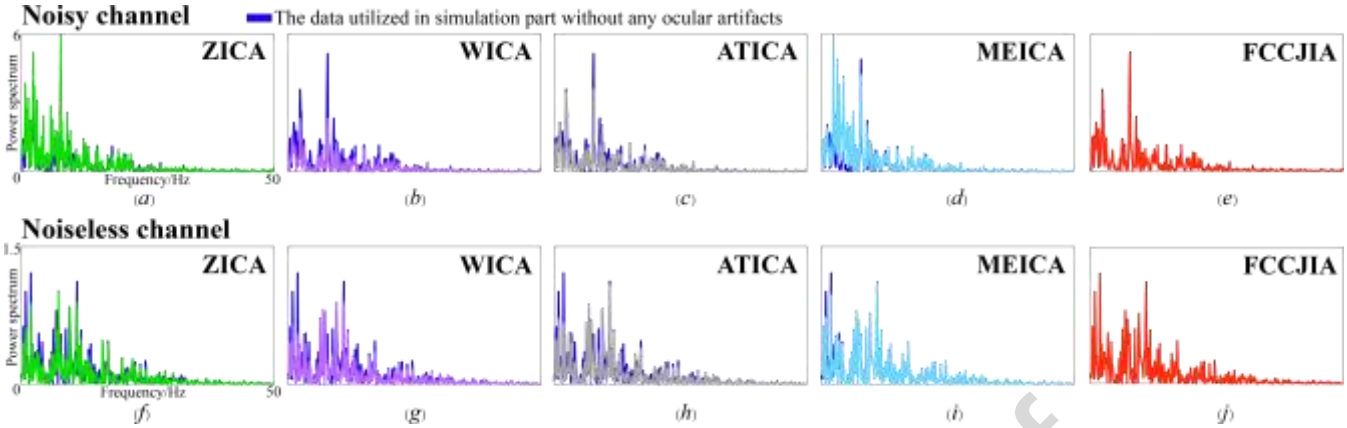

Fig. 5. the comparison of power spectral density among methods. (*a*)-(*e*) were the power spectral density comparison diagram under noisy channel calculated by ZICA, WICA, ATICA, MEICA and FCCJIA, respectively; (*f*)-(*j*) were the power spectral density comparison diagram under noiseless channel calculated by ZICA, WICA, ATICA, MEICA and FCCJIA, respectively.

B. Real EEG applications

In this section, the main objective was to evaluate the performance of different denoising methods (i.e., ZICA, WICA, ATICA, MEICA, FCCJIA) for removing ocular artifacts from resting-state EEG dataset and emotional dataset that contained prominent ocular artifacts. Fig. 6 displayed a sample of the noisy resting-state EEGs that was used for the performance comparison among the different methods.

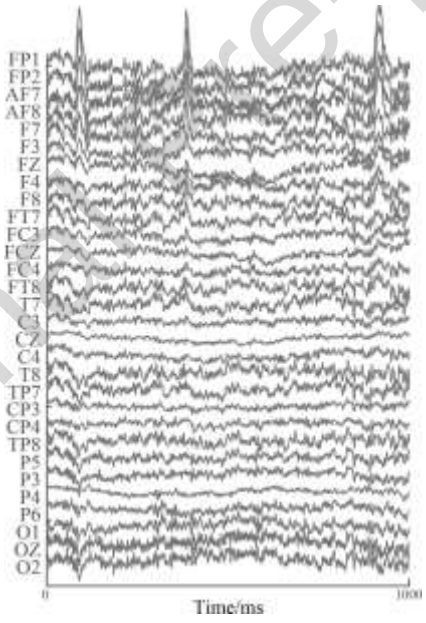

Fig. 6. the EEG segment that contained ocular artifacts.

B.1. Results of resting-state data

The simulations had provided convincing results to verify the superior performance of the proposed method under complex noises. Similarly, there were also many ocular artifacts within real EEGs that disturbed the reliability of neural analysis. Therefore, we systematically analyzed the performances of different methods by calculating relevant evaluation indices. In total, 33 trials of EEG signals with obvious ocular artifacts were adopted for comparison. It was worth noting that the prefrontal cortex was the most polluted area by ocular artifacts (referred to Fig. 6 and Fig.7 (*a*)), in which the higher amplitudes would influence the reliability of subsequent EEG-based analysis [1, 2, 35]. Additionally, regions in the back of the brain would be slightly less affected than front regions.

Specifically, Fig. 7 showed the denoising performances of different methods under the noisy channel and noiseless channel respectively. Obviously, the proposed method removed the ocular artifact components more effectively than others that illustrated in Fig. 7. Furthermore, the proposed method showed less information loss within noiseless channels located in the posterior region of the cerebral cortex. Consistently, Table V further quantitatively demonstrated its superior performance, where the average results of FCCJIA for 11 regions were better than the others, regardless of whether the channels were influenced by artifacts or not. Therefore, the results in real EEG applications were similar to those observed in simulations. Overall, based on the denoising effect of the proposed method, it was observed that channels located in the prefrontal cortex

exhibited more consistent data recovery performance with those noiseless channels.

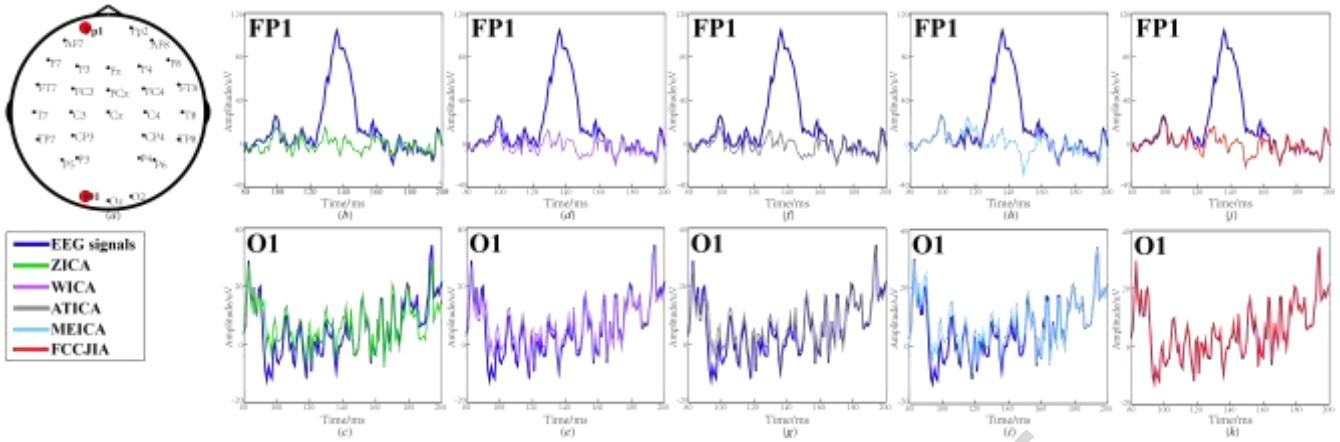

Fig. 7. The local comparisons of the EEG ocular artifacts removing among methods. (*a*) denotes the spatial location of the selected channel; (*b*)-(*c*) represent denoising performance by ZICA within the noisy channel and noiseless channel respectively; (*d*)-(*e*) represent denoising performance by WICA within the noisy channel and noiseless channel respectively; (*f*)-(*g*) represent denoising performance by ATICA within the noisy channel and noiseless channel respectively; (*h*)-(*i*) represent denoising performance by MEICA within the noisy channel and noiseless channel respectively; (*j*)-(*k*) represent denoising performance by FCCJIA within the noisy channel and noiseless channel respectively.

TABLE V
THE RESULT COMPARISONS OF DENOISING PERFORMANCE FOR BRAIN REGIONS

		ZICA	WICA	ATICA	MEICA	FCCJIA
MI	Frontal parietal (FP)	0.81±0.12∗	0.85±0.11∗	1.05±0.13∗	0.95±0.15∗	**1.12±0.29**
	Anterior Frontal (AF)	0.87±0.12∗	0.97±0.16∗	1.14±0.14∗	1.02±0.14∗	**1.27±0.31**
	Frontal (F)	0.95±0.15∗	1.13±0.17∗	1.31±0.16∗	1.16±0.15∗	**1.69±0.30**
	Frontal Temporal (FT)	1.00±0.15∗	1.21±0.20∗	1.39±0.19∗	1.25±0.19∗	**1.97±0.43**
	Frontal Central (FC)	0.99±0.14∗	1.21±0.19∗	1.41±0.20∗	1.23±0.17∗	**1.86±0.36**
	Temporal (T)	1.07±0.18∗	1.31±0.20∗	1.51±0.18∗	1.32±0.17∗	**2.08±0.43**
	Central (C)	1.02±0.11∗	1.23±0.19∗	1.45±0.17∗	1.28±0.14∗	**1.99±0.35**
	Temporal Parietal (TP)	1.05±0.13∗	1.25±0.20∗	1.44 ±0.15∗	1.26±0.14∗	**1.96±0.35**
	Central Parietal (CP)	1.03±0.14∗	1.25±0.18∗	1.47±0.15∗	1.31±0.14∗	**1.98±0.37**
	Parietal (P)	1.06±0.10∗	1.27±0.18∗	1.49±0.17∗	1.31±0.15∗	**2.00±0.37**
	Occipital (O)	1.00±0.14∗	1.21±0.25∗	1.42±0.23∗	1.28±0.18∗	**1.98±0.38**
	MEAN	0.99±0.08	1.17±0.14	1.37±0.15	1.22±0.13	**1.81±0.32**
CC	Frontal parietal (FP)	0.63±0.09∗	0.63±0.10	0.69±0.09	**0.71±0.08**	0.69±0.13
	Anterior Frontal (AF)	0.69±0.08∗	0.71±0.10∗	0.75±0.08	**0.76±0.08**	**0.76±0.12**
	Frontal (F)	0.81±0.04∗	0.84±0.05∗	0.87±0.04∗	0.86±0.04∗	**0.92±0.05**
	Frontal Temporal (FT)	0.84±0.04∗	0.88±0.05∗	0.91±0.03∗	0.90±0.04∗	**0.96±0.04**
	Frontal Central (FC)	0.84±0.04∗	0.88±0.05∗	0.91±0.04∗	0.89±0.04∗	**0.95±0.04**
	Temporal (T)	0.87±0.04∗	0.92±0.04∗	0.94±0.02∗	0.92±0.03∗	**0.98±0.03**
	Central (C)	0.85±0.03∗	0.90±0.04∗	0.92±0.03∗	0.91±0.03∗	**0.97±0.03**
	Temporal Parietal (TP)	0.88±0.03∗	0.91±0.03∗	0.94±0.02∗	0.93±0.03∗	**0.98±0.03**
	Central Parietal (CP)	0.86±0.03∗	0.91±0.04∗	0.93±0.02∗	0.92±0.03∗	**0.97±0.03**
	Parietal (P)	0.87±0.02∗	0.91±0.03∗	0.94±0.02∗	0.92±0.02∗	**0.97±0.04**
	Occipital (O)	0.85±0.04∗	0.89±0.06∗	0.92±0.04∗	0.91±0.03∗	**0.97±0.03**
	MEAN	0.82±0.08	0.85±0.09	0.88±0.08	0.87±0.07	**0.92±0.10**

B.2. Results of emotional data

In addition to those two indicators, the study also presented the classification results of each subject in Table VI. Building on the excellent performance of the proposed method in the simulation study and resting state EEG analysis, we further evaluated its effectiveness in EEG-based emotion recognition. The results of emotion recognition for different subjects were shown in Table VI. As can be seen, for almost all subjects, the classification accuracies of FCCJIA were superior to those of other methods. Additionally, the confusion matrices illustrated in Fig. 8 further revealed the robustness of FCCJIA to ocular artifact removal, as the diagonal values that related to three emotional states in the confusion matrix of the proposed method were higher than those of other methods. Compared with other state-of-the-art artifact removal methods, our proposed method demonstrated competitive performance.

TABLE VI
THE EMOTION CLASSIFICATION ACCURACIES (%) FOR SUBJECT

	Sub-1	*Sub*-2	*Sub*-3	*Sub*-4	*Sub*-5	*Sub*-6	*Sub*-7	*Sub*-8	*Sub*-9	MEAN
Original EEG	47.22	61.67	67.78	56.11	57.78	53.33	77.78	46.11	**54.44**	58.02±9.97
ZICA	39.44	48.89	61.11	51.67	57.78	52.78	73.89	42.22	46.67	52.17±10.51
WICA	52.22	65.56	57.78	56.67	63.33	51.11	80.00	48.89	51.67	58.58±9.83
ATICA	48.89	56.67	63.33	53.89	64.44	50.00	77.78	44.44	52.22	56.85±10.20
MEICA	48.89	60.56	66.67	52.78	63.33	51.67	79.44	45.56	51.11	57.78±10.74
FCCJIA	**60.00**	**67.78**	**70.00**	**60.00**	**66.67**	**56.67**	**80.56**	**49.44**	**54.44**	**62.84**±9.41

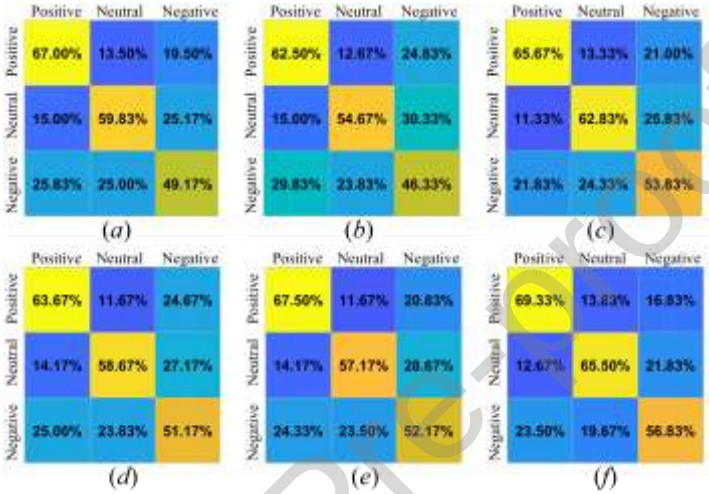

Fig. 8. The confusion matrices of different methods for **Dataset-2**. (*a*) the classification confusion matrix estimated from original EEG; (*b*)-(*f*) the classification confusion matrices estimated from EEGs preprocessed by ZICA, WICA, ATICA, MEICA, FCCJIA, respectively.

4.Discussion

With the increasing requirement of robust EEG analysis, the quality enhancement of neuronal signals preprocessing has gained much attention [47-49]. Therefore, many researchers have discussed how to remove the ocular artifacts in neural signals accurately [1, 9, 47, 50, 51]. Among various artifact removal methods, BSS showed promising performance [1, 19, 21], but how to effectively remove ocular artifacts from the EEGs and reduce the loss of normal neural information was still worth studying and exploring. Therefore, considering the successful application of CCA and ICA in artifact removal, we introduced and validated a robust adaptive ocular artifact removal method that combined CCA with ICA, while identifying the noisy channel selection and denoising analysis automatically. In general, both simulations and real EEG applications completed in this paper verified the effectiveness of the proposed method for ocular artifact removal.

To verify the robustness of the proposed method, simulation experiments were conducted with two types of noise under different artifact conditions. Firstly, outlier noise was added to the simulated data to preliminarily verify the effectiveness of the FCCJIA denoising method, as outliers and ocular artifacts had similar non-Gaussian distribution properties [2]. Subsequently, ocular artifact was introduced to further analyze the robustness of the proposed method under more complex conditions, making the simulation experiments more closely approximate the real EEG application environment. Tables I to IV consistently revealed that the data recovered by the proposed method showed better denoising performance and smaller bias between the expected data and recovered ones when compared to other four methods, whether in outliers or ocular artifacts. The smaller bias of RMSE also resulted in the significant improvement of SNR than others, whose results had been shown in Tables I to IV. In fact, the reliably recovered signal depended on the successful separation between noises and normal components, but most of the existing methods took all component vectors into account in the process of denoising [1, 3, 6], which would cause the loss of information to some degree. Therefore, we developed a novel framework by considering the shortcomings of these methods. In essence, the proposed method combined ICA and CCA to enhance the blind source separation effect. In addition, we also introduced the higher-order features to identify the noisy component vectors, while EMD and ICA-based wavelet denoising were also utilized to those selected channels for denoising analysis. Intuitively, Fig. 4 represented the data recovery performance of different methods. We could see that the proposed method held the best denoising performance under the noisy channel due to the better separation effect between noises and normal components, and showed the best fitting result within the noiseless channel which was caused by the component channel selection strategy. In addition, the proposed method maintains the best denoising performance under the noisy channel and shows the best fitting results under the noise-free channel due to the better separation between noise and normal components, which was

caused by the component channel selection strategy. This effect was further demonstrated in the power spectral density comparison plot in Fig. 5, where the power spectral density of the data recovered by FCCJIA under the noisy channel in Fig. 5 (*a*)-(*e*) exhibited frequency-domain waveforms most similar to the expected signal, while retaining more normal signal components under the noiseless channel (referred to Fig. 5 (*f*)-(*g*))). In contrast, ZICA, WICA, and ATICA inevitably resulted in component loss because they processed all component channels, while although MEICA included a noise channel selection strategy, its blind source separation strategy could not achieve better noise separation, leading to subsequent noise identification errors. Moreover, the results in Fig. 5 further validated those in Fig. 4. Overall, the results in Figs. 4 and 5 verified the better results in Tables I to IV. It is noteworthy that we provided corresponding result comparisons in *Appendix. A* to discuss the denoising effect of FCCJIA under high-frequency noise. We found that even under a high-frequency noise environment, FCCJIA still exhibited significant performance improvement compared to other methods. However, we also observed that the denoising performance of ATICA decreased with the increase of noise frequency, which was because the noise identification of ATICA was essentially based on clustering algorithms. The high proportion of artifacts directly affected its judgment of noise components, resulting in incorrect identification of artifact components.

For real EEG applications, one crucial thing for ocular artifacts denoising is to locate the noises' location accurately [1]. Simultaneously, the front regions in the brain were seriously influenced by the ocular artifacts, whereas the back regions were largely unaffected (referred to Fig. 6 and Fig. 7 (*a*)). Consequently, it was necessary to use some threshold strategies to realize the precise localization of noise components and noisy channels [1, 3, 6]. In fact, there were some features adopted to determine the noise channels [3, 9, 52]. These mentioned strategies reduced the loss of normal information certainly, but it wasn't able to satisfy the high requirement for more precise analysis of EEG applications. Considering that the high efficiency of CCA in blind source separation, the higher-order features in channel selection and the EMD-based single channel decomposition, we developed a novel method which jointly consider CCA and ICA, and further achieved the noisy channel selection automatically. Our method robustness to ocular artifacts had been quantitatively validated through simulation experiments.

To evaluate the effectiveness of the proposed method for real EEG applications, we adopted resting-state EEG segments containing obvious ocular artifacts and two commonly used indexes to evaluate the denoising performance [1, 3]. Fig. 7 showed that the proposed method yielded the best denoising and fitting performance for data recovery, regardless of the front or back regions of the brain. Similarly, Table V indicated that almost all regions calculated by FCCJIA showed significant improvements compared to other methods. Conversely, methods such as ZICA, WICA, and ATICA exhibited worse fitting performance on the noiseless channel (referred to Fig. 7 (*c*), (*e*), (*g*), (*i*) and Table V), possibly due to their failure to preserve important components for each channel. Moreover, the better performance of FCCJIA in artifact removal resulted in better emotion recognition accuracy. As shown in Table VI and Fig. 8, FCCJIA achieved the best classification accuracies for both overall classification results and the results (refer to Table VI) of three types of emotional state (refer to Fig. 8). These results further demonstrated the reliability and robustness of the proposed method. Therefore, based on the results of emotion recognition experiments designed in our current and previous studies [2, 53], we could concluded that ocular artifacts would damage the reliability of cognition-related components that were important for neural analysis and further reduced the classification accuracy of emotion recognition. Overall, FCCJIA could serve as a reference approach for EEG preprocessing that utilized in emotion analysis.

In general, the proposed method was able to effectively remove the components of artifacts and preserve more neural activity related information. However, it should be noted that the threshold strategy used in wavelet component selection, might have raised error judgements when the wavelet decomposition failed [1]. In addition, the proposed method for removing muscle artifacts from EEG signals might face limitations due to the unique characteristics of muscle artifacts. Although combining CCA and ICA could have improved the accuracy and robustness of separating normal components and artifacts in EEG signals by utilizing both correlation and independence information, there were some limitations in further ICA analysis of the components obtained from CCA, especially in the component extraction of muscle artifacts. The limitations primarily revolve around the non-Gaussian distribution assumption needed for ICA, which is one of the foundations for effective blind source separation using ICA [23-25]. However, the Gaussian distribution of muscle artifacts could have caused ICA to fail to correctly separate them, which suggested that the method proposed in the paper might not have been entirely effective in separating and removing the muscle artifact component from EEG signals, that is the Gaussian distribution of muscle artifacts could have hindered the effectiveness of ICA in correctly separating them. In essence, the crucial step of our proposed method is to locate the source of ocular artifacts. Through our previous studies[2], we revealed the relationship between ocular artifacts and outliers and utilized the higher-order statistics to identify the sources of ocular artifacts and use EMD and wavelet denoising to restrict them. In fact, this strategy is also suitable for the removal of other noise such as muscle artifacts, when their distribution priors are further extracted. As a result, the introduction of robust prior distribution that relevant to muscle artifacts, could have been more effective in removing muscle artifacts from EEG signals. In the future work, we will try to introduce some novel threshold chosen strategies or utilize the alternative techniques to achieve more effective in removing artifacts from EEG signals.

5.Conclusion

In conclusion, we have proposed FCCJIA, a novel method for automatically identifying noisy channels and removing ocular artifact components within them. The method combines CCA with ICA, which improves the separability between

artifacts and normal components, making it suitable for denoising EEG recordings with fewer channels. Our simulation and real EEG application results demonstrate that FCCJIA outperforms traditional and advanced methods, providing better ocular artifact removal and normal component preservation. Overall, the proposed method significantly improves EEG signal quality and enhances the accuracy of emotion recognition. Future research directions include exploring alternative techniques to improve the removal of muscle artifacts and further optimizing the proposed method by introducing more threshold strategies.

6.Acknowledgement

This work was supported by the STI 2030 Major Projects 2022ZD0211400 (H.C.), the National Natural Science Foundation of China (#62171074 and #61901077), the Natural Science Foundation of Chongqing (CSTB 2022NSCQ-MSX1171 and CSTB2022NSCQ-MSX0291) and the Scientific and Technological Research Program of Chongqing Municipal Education Commission KJQN202200640.

Appendix.

Appendix. A

To quantitatively evaluate the performance of our proposed method in removing ocular artifacts under higher frequencies, we extended the frequency range of the noise from 0.4 %-0.8 % to 1.2 %-1.6 %. This expansion ensured the reliability and accuracy of our proposed method. Additionally, we analyzed the performance difference between two types of noises, namely, outliers and extracted ocular artifacts. The specific noise conditions were described as follows.

Noise Condition-the influence of noise occurrence rates

We increased the occurrence rates from 1.2 %~1.6 % with a step size of 0.1 %, and the number of contaminated time series was defined as 4. Especially, the outlier intensity was defined as 20 times the maximum amplitude in the corresponding time series.

In summary, our simulations followed the methodology described in the paper, that is the operation about two types of noise addition could be described as the following.

- ***Noise category***-*Outlier addition*

$$X_{k,i}^{noise} = X_{k,i} + \varepsilon_{k,i}, \varepsilon_{k,i} \sim \begin{cases} N\left(20 \cdot \mathrm{var}\left(X_{k,\cdot}\right), 1\right), w.p.\ OR \\ N\left(0,0\right) \quad , w.p.\ 1-OR \end{cases} \tag{A1}$$

where $X_{k,i}^{noise}$ indicated the noisy data after artifacts addition for *k*-th time series at time point *i*, $X_{k,i}$ denoted the collected data without outliers, $\varepsilon_{k,i}$ represented the additional noises of outlier.

- ***Noise category***-*Ocular artifact addition*

$$X_{k,i\to i+24}^{noise} = X_{k,i\to i+24} + \Sigma, \Sigma \sim \begin{cases} OcularArtifact, w.p.\ OR \\ 0 \quad , w.p.\ 1-OR \end{cases} \tag{A2}$$

where $X_{k,i\to i+24}^{noise}$ indicated the noisy data after artifacts addition for *k*-th time series within the time period from *i* to *j*, $X_{k,i\to i+24}$ denoted the collected data without ocular artifacts, $\Sigma \in R^{1\times 25}$ represented the additional ocular artifacts.

To better simulate real ocular artifacts, the channel contaminated by ocular artifacts (denoted by *k*) was limited to only the anterior channels, and the appearance of ocular artifacts in the time series (denoted by *i*) was unknown and random.

Step-1: Simulated different noise conditions as mentioned before, i.e., 1) the influence of higher noise occurrence rates.

Step-2: Removed the ocular artifacts by methods.

Step-3: Evaluated the performance by the following indexes among methods, which included:

- ***Index***-1: Computed the SNR as the following formula [1-3]

$$SNR = \frac{1}{Ch} \cdot \sum_{k=1}^{Ch} 10 \cdot log \frac{\sum_{i=1}^{N} \left(X_{k,i}^{exp}\right)^2}{\sum_{i=1}^{N} \left(X_{k,i}^{exp} - X_{k,i}^{rec}\right)^2} \tag{A3}$$

- ***Index***-2: Computed the RMSE between recovered data by methods and expected data [4, 5].

$$RMSE = \frac{1}{Ch} \cdot \sum_{k=1}^{Ch} \sqrt{\frac{1}{N} \cdot \sum_{i=1}^{N} \left(X_{k,i}^{exp} - X_{k,i}^{rec}\right)^2} \tag{A4}$$

where X^{exp} denoted the expected data and X^{rec} denoted the recovered data by methods.

Step-4: Repeated **Step**s **1-3** 100 times under noise conditions to reveal the differences by paired-*t* test [6, 7].

Basically, in this simulation experiment we revealed the denoising performance differences among methods under higher noise occurrence rates. Tables A1 to A2 integrated these experimental results, where the value marked with bold font style indicated the best result and "*" mean the significant difference between our proposed method and the others. Through Table A1 to A2 we could see that all the two indexes (SNR and EMSE) of FCCJIA were almost better than others, which quantitatively revealed the significant improvement on artifacts removal and indirectly proved the robustness of our

proposed method.

TABLE A1
RESULTS COMPARISON WITH INCRASING OCCURRENCE FREQUENCIES OF OUTLIERS

	Frequency of outliers									
	1.2%	1.3%	1.4%	1.5%	1.6%	1.2%	1.3%	1.4%	1.5%	1.6%
	Index value of SNR					Index value of RMSE				
ZICA	9.63 ±1.25*	9.68 ±1.21*	9.79 ±1.25*	9.57 ±1.26*	9.35 ±1.20*	1.14 ±0.54*	1.21 ±0.63*	1.15 ±0.59*	1.26 ±0.62*	1.39 ±0.64*
WICA	7.02 ±1.22*	7.17 ±1.38*	6.98 ±1.18*	7.10 ±1.39*	7.21 ±1.17*	1.00 ±0.12*	1.03 ±0.14*	1.03 ±0.14*	1.02 ±0.13*	1.03 ±0.14*
ATICA	8.81 ±1.62*	8.76 ±1.89*	8.70 ±1.70*	8.44 ±1.92*	8.92 ±1.59*	0.83 ±0.18*	0.87 ±0.18*	0.87 ±0.22*	0.89 ±0.17*	0.87 ±0.23*
MEICA	13.19 ±2.48*	12.74 ±3.04*	13.33 ±2.75*	13.26 ±2.93*	12.65 ±2.90*	3.38 ±0.94*	3.77 ±1.17*	3.58 ±1.03*	3.84 ±1.19*	4.08 ±1.21*
FCCJIA	**33.73 ±4.17**	**32.82 ±3.57**	**33.68 ±4.29**	**33.74 ±3.75**	**33.84 ±3.61**	**0.22 ±0.53**	**0.31 ±0.81**	**0.41 ±1.09**	**0.35 ±0.89**	**0.35 ±0.83**

TABLE A2
RESULTS COMPARISON WITH INCRASING OCCURRENCE FREQUENCIES OF OCULAR ARTIFACTS

	Frequency of ocular artifacts									
	1.2%	1.3%	1.4%	1.5%	1.6%	1.2%	1.3%	1.4%	1.5%	1.6%
	Index value of SNR					Index value of RMSE				
ZICA	7.18 ±0.50*	6.94 ±0.46*	7.03 ±0.50*	6.84 ±0.44*	6.86 ±0.51*	4.12 ±0.23*	4.38 ±0.17*	4.40 ±0.16*	4.72 ±0.15*	4.86 ±0.17*
WICA	6.03 ±1.18*	5.81 ±1.29*	5.93 ±1.34*	5.28 ±1.03*	5.00 ±1.31*	1.41 ±0.46*	1.38 ±0.25*	1.48 ±0.45*	1.79 ±0.51*	2.29 ±0.73*
ATICA	7.05 ±1.42*	6.33 ±1.31*	6.35 ±1.44*	5.74 ±1.11*	5.60 ±1.40*	1.69 ±0.95*	2.57 ±1.33*	2.31 ±1.17*	3.29 ±1.43*	3.54 ±1.28*
MEICA	11.19 ±1.99*	11.53 ±2.03*	11.03 ±2.25*	10.83 ±1.91*	10.07 ±2.15*	2.47 ±0.24*	2.57 ±0.23*	2.65 ±0.35*	3.03 ±0.61*	3.48 ±0.72*
FCCJIA	**16.18 ±4.25**	**14.50 ±3.69**	**15.04 ±3.66**	**13.07 ±2.49**	**12.23 ±3.42**	**0.80 ±0.31**	**0.90 ±0.23**	**0.93 ±0.34**	**1.26 ±0.46**	**1.84 ±0.73**

Appendix. B

To quantify the feasibility of the method in online experiments, we designed a simulation experiment to compare the time consumption of different methods. In this experiment, we used ocular artifacts as the added noise type, which was described in detail as follows.

Noise Condition

The occurrence rate of ocular artifacts was defined as 1.2 %, the number of contaminated time series was defined as 4.

In summary, the addition method of EEG artifact was as the following:

$$X_{k,i\to i+24}^{noise} = X_{k,i\to i+24} + \Sigma, \Sigma \sim \begin{cases} OcularArtifact, w.p.\ OR \\ 0 \quad\quad , w.p.\ 1-OR \end{cases} \tag{B1}$$

where $X_{k,i\to i+24}^{noise}$ indicated the noisy data after artifacts addition for *k*-th time series within the time period from *i* to *j*, $X_{k,i\to i+24}$ denoted the collected data without ocular artifacts, $\Sigma \in R^{1\times 25}$ represented the additional ocular artifacts.

In current study, we mainly utilized the EEGs recorded in the channels of frontal aera, because this aera has been reported to be seriously influenced by ocular artifacts [28-31]. Specifically, the channels to add simulated ocular artifacts were randomly selected and the occurrence of the ocular artifacts is also set randomly.

Step-1: Simulated different noise conditions as mentioned in ***Noise Condition***

Step-2: Removed the ocular artifacts by methods.

Step-3: Evaluated the performance by the following indexes among methods, which included:

• ***Index***-1: Computed the SNR as the following formula [1-3]

$$SNR = \frac{1}{Ch} \cdot \sum_{k=1}^{Ch} 10 \cdot log \frac{\sum_{i=1}^{N} \left(X_{k,i}^{exp} \right)^2}{\sum_{i=1}^{N} \left(X_{k,i}^{exp} - X_{k,i}^{rec} \right)^2} \tag{B2}$$

• ***Index***-2: Computed the RMSE between recovered data by methods and expected data [4, 5].

$$RMSE = \frac{1}{Ch} \cdot \sum_{k=1}^{Ch} \sqrt{\frac{1}{N} \cdot \sum_{i=1}^{N} \left(X_{k,i}^{exp} - X_{k,i}^{rec} \right)^2} \tag{B3}$$

where X^{exp} denoted the expected data and X^{rec} denoted the recovered data by methods.

• ***Index***-3: Computed the time consumption (TC) for artifact removal.

$$TC = Time_{End} - Time_{Begin} \tag{B4}$$

where $Time_{Begin}$ represented the start time and $Time_{End}$ represented the end time of the algorithm calculation.

Step-4: Repeated **Step**s **1-3** 100 times under noise conditions to reveal the differences by paired-*t* test [6, 7].

In this simulation experiment, we revealed the average time consumption and corresponding metrics of different methods for 100 runs. The values marked in bold indicated the best results, and "*" represented significant differences between the proposed method and other methods. From Table B1, we could see that FCCJIA significantly improved computational efficiency compared to WICA and ATICA. Meanwhile, considering the drawbacks of ZICA and MEICA in denoising performance and the widespread application of WICA in signal preprocessing, we believed that FCCJIA provided a more reliable approach for online processing of EEG signals.

TABLE B1

COMPARISON RESULTS UNDER OCULAR ARTIFACTS INFLUENCE FOR FIVE METHODS

	ZICA	WICA	ATICA	MEICA	FCCJIA
SNR	7.18±0.50*	6.03±1.18*	7.05±1.42*	11.19±1.99*	**16.18±4.25**
RMSE	4.12±0.23*	1.41±0.46*	1.69±0.95*	2.47±0.24*	**0.80±0.31**
TC	**0.14±0.12**	2.08±0.60*	20.04±3.34*	0.22±0.26	0.71±0.31

Appendix. C

To quantitatively evaluate the impact of different time window lengths, we designed corresponding simulation experiments using noise-free data identical to that used in the paper. To facilitate the selection of different time windows, we first truncated the data and then added ocular artifacts noise. In terms of data truncation, we compared and discussed the RMSE performance indicators of various methods under different time windows, ranging from 100 to 1000 with a step size of 20. Next, we added ocular artifacts to data of different lengths. In this experiment, we used ocular artifacts as an additional noise type and set the number of channels affected by ocular artifacts noise to 6. It was worth noting that when the noise frequency was 0.3% while the data segment length was less than 340, the actual number of noise occurrences was not 1. Therefore, to solve this problem, we fixed the number of ocular artifacts noise occurrences to 3 times and randomized their occurrence positions.

In summary, the corresponding noise settings of the simulation experiment were as follows: ocular artifacts were added as noise types, the number of ocular artifacts occurrences was set to 3, and the number of affected channels was 6. The resulting RMSE-time window change curve was shown in Fig. C1.

It was observed from Fig. C1 that when the data segment length exceeded 400 data points, the RMSE values of various methods began to stabilize, which indicated that a time window length greater than 400 was an appropriate length. This also confirmed that the 1000-time window length we used in our study was appropriate.

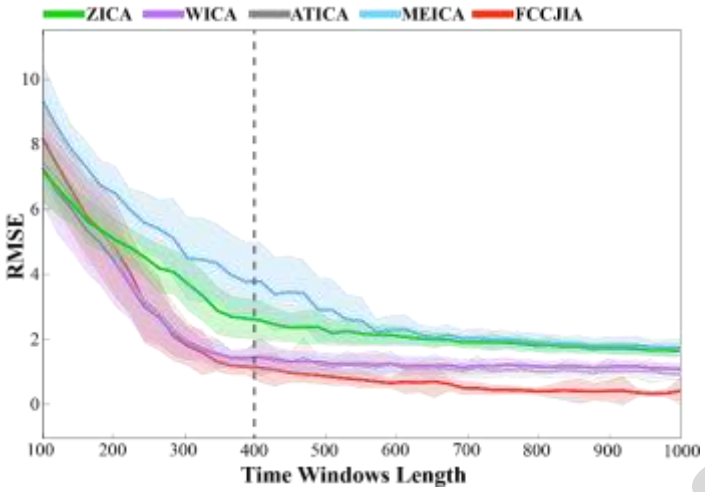

Fig. C1. Comparison of the results between the methods based on RMSE metric under different time window lengths. The solid line represents the mean value and the semi-transparent line represents the variance value.

References

[1] P. LI, X. GAO, P. ZHU, W. HUANG *et al.*, "An Adaptive EOG Removal Method Based on Local Density," *Journal of Electronics & Information Technology,* vol. 44, no. 2, pp. 464-476, 2022.

[2] X. Gao, W. Huang, Y. Liu, Y. Zhang *et al.*, "A novel robust Student's t-based Granger causality for EEG based brain network analysis," *Biomedical Signal Processing Control,* vol. 80, p. 104321, 2023.

[3] R. Mahajan and B. I. Morshed, "Unsupervised eye blink artifact denoising of EEG data with modified multiscale sample entropy, kurtosis, and wavelet-ICA," *IEEE Journal of Biomedical and Health Informatics,* vol. 19, no. 1, pp. 158-165, 2014.

[4] J. Gotman, D. R. Skuce, C. J. Thompson, P. Gloor *et al.*, "Clinical applications of spectral analysis and extraction of features from electroencephalograms with slow waves in adult patients," *Electroencephalography Clinical Neurophysiology,* vol. 35, no. 3, pp. 225-235, 1973.

[5] A. De Cheveigné and J. Z. Simon, "Denoising based on time-shift PCA," *Journal of neuroscience methods,* vol. 165, no. 2, pp. 297-305, 2007.

[6] N. P. Castellanos and V. A. Makarov, "Recovering EEG brain signals: Artifact suppression with wavelet enhanced independent component analysis," *Journal of neuroscience methods,* vol. 158, no. 2, pp. 300-312, 2006.

[7] S. Çınar, "Design of an automatic hybrid system for removal of eye-blink artifacts from EEG recordings," *Biomedical Signal Processing Control,* vol. 67, p. 102543, 2021.

[8] M. Manojprabu and V. S. Dhulipala, "Power aware hessian multi-set canonical correlations based algorithm for wireless eeg sensor networks," *Wireless Personal Communications,* vol. 117, pp. 2745-2756, 2021.

[9] A. K. Maddirala and K. C. Veluvolu, "ICA with CWT and k-means for Eye-blink Artifact Removal from Fewer Channel EEG," *IEEE Transactions on Neural Systems Rehabilitation Engineering,* 2022.

[10] A. Goldental, R. Vardi, S. Sardi, P. Sabo *et al.*, "Broadband macroscopic cortical oscillations emerge from intrinsic neuronal response failures," *Frontiers in neural circuits,* vol. 9, p. 65, 2015.

[11] M. Moutoussis, M. W. Orrell, and R. Morris, "Modeling discoordination of cortical neuroactivity: relevance for the executive control of attention in Alzheimer's disease," *Journal of Integrative Neuroscience,* vol. 3, no. 01, pp. 85-104, 2004.

[12] X. Chen, X. Xu, A. Liu, M. J. McKeown *et al.*, "The use of multivariate EMD and CCA for denoising muscle artifacts from few-channel EEG recordings," *IEEE transactions on instrumentation measurement,* vol. 67, no. 2, pp. 359-370, 2017.

[13] J. A. Mucarquer, P. Prado, M.-J. Escobar, W. El-Deredy *et al.*, "Improving EEG muscle artifact removal with an EMG array," *IEEE transactions on instrumentation measurement,* vol. 69, no. 3, pp. 815-824, 2019.

[14] P. Gajbhiye, R. K. Tripathy, A. Bhattacharyya, and R. B. Pachori, "Novel approaches for the removal of motion

artifact from EEG recordings," *IEEE Sensors Journal*, vol. 19, no. 22, pp. 10600-10608, 2019.

[15] S. N. A. Kordmahale, S. Kilani, Z. Ghassemlooy, Q. Wu *et al.*, "A novel artifact removal method for the SSVEP signal using hybrid CCA-DWT and comparative analysis for feature selection and classification in the P300 signal," in *2022 13th International Symposium on Communication Systems, Networks and Digital Signal Processing (CSNDSP)*, 2022, pp. 390-394: IEEE.

[16] C. Kaur, A. Bisht, P. Singh, and G. Joshi, "EEG Signal denoising using hybrid approach of Variational Mode Decomposition and wavelets for depression," *Biomedical Signal Processing Control*, vol. 65, p. 102337, 2021.

[17] R. B. Satpathy and G. Ramesh, "Advance approach for effective EEG artefacts removal," *Recent Trends Advances in Artificial Intelligence Internet of Things*, pp. 267-278, 2020.

[18] Y. Gu, X. Li, S. Chen, and X. Li, "AOAR: an automatic ocular artifact removal approach for multi-channel electroencephalogram data based on non-negative matrix factorization and empirical mode decomposition," *Journal of Neural Engineering*, vol. 18, no. 5, p. 056012, 2021.

[19] D. Safieddine, A. Kachenoura, L. Albera, G. Birot *et al.*, "Removal of muscle artifact from EEG data: comparison between stochastic (ICA and CCA) and deterministic (EMD and wavelet-based) approaches," *EURASIP Journal on Advances in Signal Processing*, vol. 2012, no. 1, pp. 1-15, 2012.

[20] A. Duggento, M. Bianciardi, L. Passamonti, L. L. Wald *et al.*, "Globally conditioned Granger causality in brain–brain and brain–heart interactions: a combined heart rate variability/ultra-high-field (7 T) functional magnetic resonance imaging study," *Philosophical Transactions of the Royal Society of London, Series A: Mathematical, Physical and Engineering Sciences*, vol. 374, no. 2067, p. 20150185, 2016.

[21] X. Chen, Q. Chen, Y. Zhang, and Z. J. Wang, "A novel EEMD-CCA approach to removing muscle artifacts for pervasive EEG," *IEEE Sensors Journal*, vol. 19, no. 19, pp. 8420-8431, 2018.

[22] X. Chen, H. Peng, F. Yu, and K. Wang, "Independent vector analysis applied to remove muscle artifacts in EEG data," *IEEE Transactions on Instrumentation Measurement*, vol. 66, no. 7, pp. 1770-1779, 2017.

[23] A. Hyvärinen and E. Oja, "Independent component analysis: algorithms and applications," *Neural networks*, vol. 13, no. 4-5, pp. 411-430, 2000.

[24] P. Comon, "Independent component analysis, a new concept?," *Signal processing*, vol. 36, no. 3, pp. 287-314, 1994.

[25] A. Hyvarinen, "Fast and robust fixed-point algorithms for independent component analysis," *IEEE transactions on Neural Networks*, vol. 10, no. 3, pp. 626-634, 1999.

[26] O. Dimigen, "Optimizing the ICA-based removal of ocular EEG artifacts from free viewing experiments," *NeuroImage*, vol. 207, p. 116117, 2020.

[27] A. Delorme, T. Sejnowski, and S. Makeig, "Enhanced detection of artifacts in EEG data using higher-order statistics and independent component analysis," *Neuroimage*, vol. 34, no. 4, pp. 1443-1449, 2007.

[28] T. Liu, D. J. C. m. Yao, and p. i. biomedicine, "Removal of the ocular artifacts from EEG data using a cascaded spatio-temporal processing," vol. 83, no. 2, pp. 95-103, 2006.

[29] P. Berg, M. J. E. Scherg, and c. neurophysiology, "A multiple source approach to the correction of eye artifacts," vol. 90, no. 3, pp. 229-241, 1994.

[30] C. Dora, P. K. J. B. Biswal, and B. Engineering, "An improved algorithm for efficient ocular artifact suppression from frontal EEG electrodes using VMD," vol. 40, no. 1, pp. 148-161, 2020.

[31] A. Harris, R. Adolphs, C. Camerer, and A. J. P. o. Rangel, "Dynamic construction of stimulus values in the ventromedial prefrontal cortex," vol. 6, no. 6, p. e21074, 2011.

[32] A. Abidi, I. Nouira, and M. H. Bedoui, "Parallel Implementation on GPU for EEG Artifact Rejection by Combining FastICA and TQWT," in *2018 IEEE/ACS 15th International Conference on Computer Systems and Applications (AICCSA)*, 2018, pp. 1-8: IEEE.

[33] W. Sun, Y. Su, X. Wu, and X. Wu, "A novel end-to-end 1D-ResCNN model to remove artifact from EEG signals," *Neurocomputing*, vol. 404, pp. 108-121, 2020.

[34] Z. A. A. Alyasseri, A. T. Khader, M. A. Al-Betar, A. K. Abasi *et al.*, "EEG signals denoising using optimal wavelet transform hybridized with efficient metaheuristic methods," *IEEE Access*, vol. 8, pp. 10584-10605, 2019.

[35] P. Li, C. Li, J. C. Bore, Y. Si *et al.*, "L1-norm based time-varying brain neural network and its application to dynamic analysis for motor imagery," *Journal of Neural Engineering*, vol. 19, no. 2, p. 026019, 2022.

[36] P. Li, X. Huang, F. Li, X. Wang *et al.*, "Robust Granger analysis in Lp norm space for directed EEG network analysis," *IEEE Transactions on Neural Systems and Rehabilitation Engineering*, vol. 25, no. 11, pp. 1959-1969, 2017.

[37] K. Liu, Q. Lai, P. Li, Z. Yu *et al.*, "Robust Bayesian Estimation of EEG-Based Brain Causality Networks," *IEEE Transactions on Biomedical Engineering*, 2022.

[38] W.-L. Zheng, J.-Y. Zhu, and B.-L. Lu, "Identifying stable patterns over time for emotion recognition from EEG," *IEEE Transactions on Affective Computing*, vol. 10, no. 3, pp. 417-429, 2017.

[39] M. Saini, U. Satija, and M. D. Upadhayay, "Wavelet based waveform distortion measures for assessment of denoised EEG quality with reference to noise-free EEG signal," *IEEE Signal Processing Letters*, vol. 27, pp. 1260-1264, 2020.

[40] S. Phadikar, N. Sinha, and R. Ghosh, "Automatic EEG eyeblink artefact identification and removal technique using independent component analysis in combination with support vector machines and denoising autoencoder," *IET Signal Processing*, vol. 14, no. 6, pp. 396-405, 2020.

[41] S. Phadikar, N. Sinha, R. Ghosh, and E. Ghaderpour, "Automatic Muscle Artifacts Identification and Removal from Single-Channel EEG Using Wavelet Transform with Meta-Heuristically Optimized Non-Local Means Filter," *Sensors*, vol. 22, no. 8, p. 2948, 2022.

[42] P. Li, H. Liu, Y. Si, C. Li *et al.*, "EEG based emotion recognition by combining functional connectivity network and local activations," *IEEE Transactions on Biomedical Engineering*, vol. 66, no. 10, pp. 2869-2881, 2019.

[43] J. Fdez, N. Guttenberg, O. Witkowski, and A. Pasquali, "Cross-subject EEG-based emotion recognition through neural networks with stratified normalization," *Frontiers in neuroscience*, vol. 15, p. 626277, 2021.

[44] C.-C. Chang and C.-J. Lin, "LIBSVM: a library for support vector machines," *ACM transactions on intelligent systems technology*, vol. 2, no. 3, pp. 1-27, 2011.

[45] S. Hwang, M. Ki, K. Hong, and H. Byun, "Subject-independent EEG-based emotion recognition using adversarial learning," presented at the International winter conference on brain-computer interface (BCI), 2020.

[46] N. Zhuang, Y. Zeng, L. Tong, C. Zhang *et al.*, "Emotion recognition from EEG signals using multidimensional information in EMD domain," *BioMed research international*, vol. 2017, 2017.

[47] L.-W. Ko, O. Komarov, W.-K. Lai, W.-G. Liang *et al.*, "Eyeblink recognition improves fatigue prediction from single-channel forehead EEG in a realistic sustained attention task," *Journal of neural engineering*, vol. 17, no. 3, p. 036015, 2020.

[48] J. Zhu, C. Yang, X. Xie, S. Wei *et al.*, "Mutual Information Based Fusion Model (MIBFM): Mild Depression Recognition Using EEG and Pupil Area Signals," *IEEE Transactions on Affective Computing*, 2022.

[49] P. Sheela and S. D. Puthankattil, "A hybrid method for artifact removal of visual evoked EEG," *Journal of Neuroscience Methods*, vol. 336, p. 108638, 2020.

[50] J. Yin, A. Liu, C. Li, R. Qian *et al.*, "Frequency Information Enhanced Deep EEG Denoising Network for Ocular Artifact Removal," *IEEE Sensors Journal*, vol. 22, no. 22, pp. 21855-21865, 2022.

[51] H. Zhang, M. Zhao, C. Wei, D. Mantini *et al.*, "Eegdenoisenet: A benchmark dataset for deep learning solutions of eeg denoising," *Journal of Neural Engineering*, vol. 18, no. 5, p. 056057, 2021.

[52] B. Wu, W. Meng, and W.-Y. Chiu, "Towards Enhanced EEG-based Authentication with Motor Imagery Brain-Computer Interface," in *Proceedings of the 38th Annual Computer Security Applications Conference*, 2022, pp. 799-812.

[53] M. Yu, S. Xiao, M. Hua, H. Wang *et al.*, "EEG-based emotion recognition in an immersive virtual reality environment: From local activity to brain network features," *Biomedical Signal Processing Control*, vol. 72, p. 103349, 2022.

Declaration of Competing Interest

The authors declare that they have no known competing financial interests or personal relationships that could have appeared to influence the work reported in this paper.

Highlights

- A novel artifact removal technology was proposed by combining the advantage of several noise restriction methods, which identified the noise component adaptively.
- The proposed method largely eliminated the component of ocular artifacts and preserved the inherent component of EEGs as many as possible.
- The proposed method significantly improved the quality of EEGs, which resulted in more reasonable spectral distribution of EEG power density for resting state and higher accuracy for emotion recognition.
- The proposed method holds smaller time consumption which is suitable for online artifact removal.